Optics Letters

Thermal noise and mechanical loss of SiO_2/Ta_2O_5 optical coatings at cryogenic temperatures

John M. Robinson,[1,*] Eric Oelker,[1] William R. Milner,[1] Dhruv Kedar,[1] Wei Zhang,[1] Thomas Legero,[2] Dan G. Matei,[2] Sebastian Häfner,[2] Fritz Riehle,[2] Uwe Sterr,[2] and Jun Ye[1]

[1]JILA, NIST and University of Colorado, 440 UCB, Boulder, Colorado 80309, USA
[2]Physikalisch-Technische Bundesanstalt, Bundesallee 100, 38116 Braunschweig, Germany
*Corresponding author: john.robinson@colorado.edu

Received 11 November 2020; revised 9 December 2020; accepted 9 December 2020; posted 10 December 2020 (Doc. ID 413758); published 25 January 2021

Mechanical loss of dielectric mirror coatings sets fundamental limits for both gravitational wave detectors and cavity-stabilized optical local oscillators for atomic clocks. Two approaches are used to determine the mechanical loss: ringdown measurements of the coating quality factor and direct measurement of the coating thermal noise. Here we report a systematic study of the mirror thermal noise at 4, 16, 124, and 300 K by operating reference cavities at these temperatures. The directly measured thermal noise is used to extract the mechanical loss for SiO_2/Ta_2O_5 coatings, which are compared with previously reported values.

https://doi.org/10.1364/OL.413758

Low mechanical loss optical coatings play a critical role in optical reference cavities [1–4], gravitational wave detectors [5], and cavity optomechanics [6]. Mechanical dissipation in the coating results in length fluctuations referred to as Brownian coating thermal noise (CTN), which can limit the precision of interferometric measurements. Thus, there has been considerable experimental effort to characterize the level of CTN present in current optical coatings.

The power spectral density (PSD) of thermal noise induced displacement fluctuations is proportional to temperature. Several gravitational wave detectors, thus plan to operate at cryogenic temperatures, including KAGRA at 20 K [7], LIGO Voyager at 124 K [8,9], and the Einstein Telescope at 10 K [10]. It is also clear that cryogenic optical cavities provide the best laser stability for optical atomic clocks [2,11]. Improving the performance of these interferometers relies upon characterizing and improving CTN at cryogenic temperatures.

There are two distinct methods for determining the Brownian CTN of an optical coating. The first is referred to as the "mechanical ringdown approach." This involves measuring the mechanical quality factor, Poisson ratio, and Young's modulus for each coating material. These mechanical properties for the coating and substrate are then used to calculate the CTN for a given mirror. This method of calculating the CTN may not account for all multilayer phenomena in the coating. The second method, referred to as a "direct measurement," determines the CTN of the coating by measuring the frequency stability of optical cavities. This approach has the challenge of extracting a coating loss angle from a single measurement over a broad frequency range, requiring input on other coating and substrate properties. Due to the challenges in each approach, it is vital both are undertaken as independent and complementary research efforts. In this Letter, we present direct CTN measurements of SiO_2/Ta_2O_5 using the most stable cavities in operation today from cryogenic to room temperatures.

Highly reflective optical coatings are made by alternating layers of high and low refractive index material. The most common choices are SiO_2 and Ta_2O_5 for the low and high refractive index, respectively. Mechanical ringdown measurements have been used to characterize both the coating materials and multilayer coatings at cryogenic temperatures. Individual thin films of SiO_2 and Ta_2O_5 have shown a peak in the mechanical loss angle at cryogenic temperatures [12,13]. A multilayer coating of $SiO_2/Ti{:}Ta_2O_5$ was measured to have a loss peak, reaching approximately 1.0×10^{-3} at $T = 20$ K [14]. Ringdown measurements of an undoped SiO_2/Ta_2O_5 coating showed a largely temperature independent mechanical loss angle of 4×10^{-4} at cryogenic temperatures [15]. The possibility of increased mechanical loss at cryogenic temperatures has motivated research in developing new optical coatings [12,16,17]. We are presenting our direct CTN measurements versus temperature to complement the growing body of CTN research.

We perform direct measurement of CTN of two independent multilayer coatings composed of SiO_2/Ta_2O_5. By employing these coatings in ultrastable rigid crystalline silicon (c-Si) Fabry–Perot cavities, we characterize the CTN around 4 K, 16 K, and 124 K. These particular temperatures are informative for future gravitational wave detectors. We also show an upper bound for a third SiO_2/Ta_2O_5 coating at room temperature, measured using an ultra-low expansion (ULE) cavity.

We study the mechanical loss of the HR coatings by measuring the noise of three independent Fabry–Perot cavities [2,4,18]. All three cavities use ion-beam-sputtered optical coatings made by Advanced Thin Films. The coatings for the cryogenic cavities have 21 layers of SiO_2 and 20 layers of Ta_2O_5, while the room

Table 1. Optical Cavity and Coating Properties

L (cm)	T (K)	d (μm)	Spacer/Sub.	ROC_1/ROC_2
6	4, 16.2	9.2	c-Si/c-Si	1 m/1 m
21	123.3	9.2	c-Si/c-Si	∞/1 m
40	288	3.8	ULE/FS	∞/1 m

Table 2. Material Properties

Material	Y (GPa)	σ	ϕ
c-Si ($\langle 111 \rangle$)	187.5 [20]	0.23 [20]	10^{-7} [21]
$SiO_2-Ta_2O_5$	91(7) [22]	0.19 [22]	[This work]
Fused silica	72 [23]	0.17 [23]	1×10^{-6} [24]
ULE	68 [25]	0.17 [25]	1.6×10^{-5} [26]

temperature system has 18 SiO_2 and 19 Ta_2O_5 layers, respectively. The coatings were deposited at room temperature and then annealed at a temperature of approximately 480° C. The physical details of the cavities are shown in Table 1, where L is the cavity length, T is the cavity temperature, d is the coating thickness, and $ROC_{1,2}$ is the radius of curvature of each mirror, respectively. We calculate individual contributions to thermal noise for each system according to the analysis in [19]. Here, noise is quantified in terms of fractional frequency PSD, which is defined as $S_y(f) = \frac{S_\nu(f)}{\nu^2}$, where $S_\nu(f)$ is the single-sided PSD of frequency fluctuations and ν is the optical frequency.

The contributions from Brownian motion of the cavity constituents and substrate thermo-elastic noise are shown in Fig. 1. We use the material properties in Table 2 and the equations in [19]. Substrate thermo-elastic noise scales with the squared power of temperature T^2 and the substrate coefficient of thermal expansion (CTE) α_{sub}^2, and is thus less than 10^{-36} Hz^{-1} at 1 Hz for our cryogenic systems [19]. Coating thermo-optic noise is 4×10^{-36} Hz^{-1} at 1 Hz for the room temperature system and is below 10^{-36} Hz^{-1} at 1 Hz for the cryogenic systems. The relative magnitude of the spacer and substrate contribution for the cryogenic silicon cavities highlights their advantage for studying the CTN, provided one operates at a temperature where the silicon CTE is Tiently small.

We first characterize the 124 K system, which has the lowest thermal noise floor as seen in Fig. 1. This system is used as the local oscillator for the JILA Sr1 optical lattice clock [27]. The laser frequency measurement comes from recording the correction signal applied to keep the laser on resonance with the clock transition. We use three independent data runs, each lasting at least 20,000 seconds. The PSD is calculated for Fourier frequencies from 3×10^{-4} to 10^{-2} Hz and is shown in Fig. 2 as the green data. These measurements are restricted to low frequencies, limited by the finite duty cycle of the clock. We also

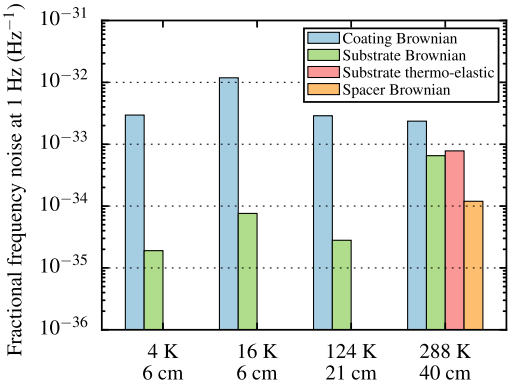

Fig. 1. Based on representative numbers from existing literature, we illustrate the major contributions to the thermal noise for three optical cavities at various temperatures and with lengths ranging from 6 to 40 cm. Fractional noise associated with coating and substrate scales inversely with the cavity length. Substrate thermo-elastic and spacer Brownian noise are below 10^{-36} Hz^{-1} for our cryogenic systems.

plot an estimate of the PSD for this system at higher frequency based on a cross-spectral density (CSD) measurement from [11].

The PSD of the 124 K system measured with the optical clock constitutes a direct measurement of its thermal noise level as the noise contribution from the clock itself is negligible [11]. We extract the CTN of the remaining systems by measuring their heterodyne beat against the 124 K system using a lambda-type zero dead time frequency counter, and subtracting its thermal noise contribution in quadrature. Since the thermal noise floors are uncorrelated, we subtract the direct measurement in quadrature from each heterodyne beat to obtain the 4 K (blue), 16 K (red), and 288 K (orange) noise PSD. The uncertainty of the fitted 124 K PSD is propagated for the subtraction.

Several authors have reported a frequency-dependent loss angle for SiO_2/Ta_2O_5 coatings [28,29]. We fit the measured spectra to the functional form of $S_y(f) = a/f^b$ in order to allow for any potential frequency dependence. A deviation from $b = 1$ for the CTN indicates a frequency-dependent loss angle. The fits to the measured spectra are shown as dashed lines in Fig. 2. We find weak dependencies on frequency as summarized in Fig. 4.

To extract a mechanical loss angle from the measured noise spectrum, we perform a characterization of all other noise sources in the reference cavity systems. The 124 K system has been thoroughly characterized as described in [30]. Since that work, we have made several improvements to the setup, including active stabilization of the transmitted optical power, active temperature control of the outermost vacuum chamber, and improved optical quality of the optics.

The technical noise budget of the 6 cm system is shown in Fig. 3(A). We show fits to the measured noise arising from temperature, Pound–Drever–Hall (PDH) servo, and the PDH photodiode (PD). The dominant technical noise source is residual amplitude modulation (RAM), shown as the red data. The sum of the technical noise is well below the measured noise.

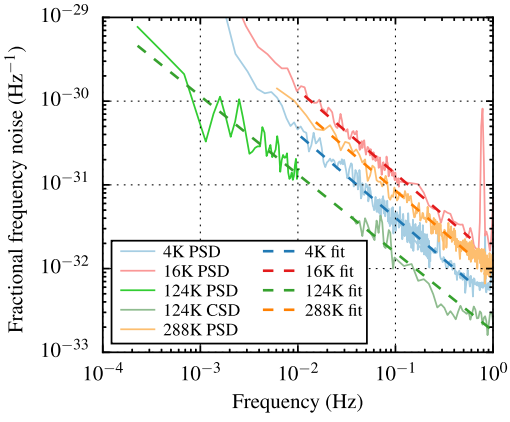

Fig. 2. Measured noise PSD at various temperatures (solid curves). The dashed lines are the fits to $S_y(f) = a/f^b$.

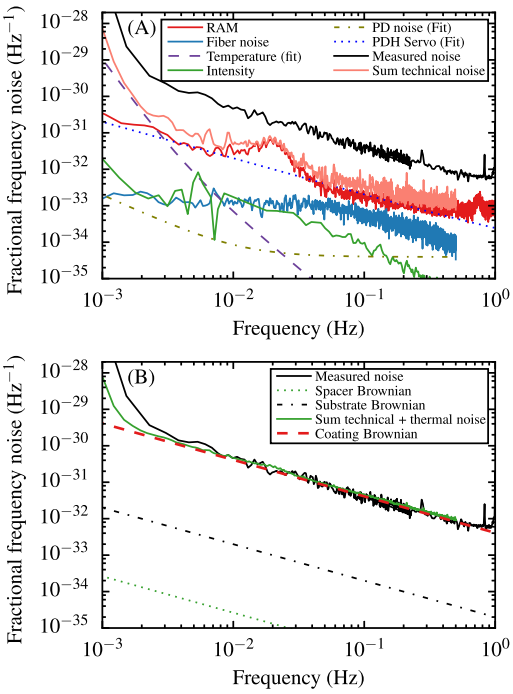

Fig. 3. (A) Technical noise contributions for the 4 K system, along with the sum of the technical noise (pink line) and the measured noise (black line). (B) Intrinsic thermal noise for the cavity, along with the sum of technical noise and thermal noise (green) and coating Brownian noise (dashed red).

Figure 3(B) shows the intrinsic thermal noise of the cavity, including Brownian noise from the spacer (dotted), substrate (dashed–dotted), and coating (dashed). The measured noise is shown (black) along with the sum of technical noise and thermal noise (green). The CTN is the dominant noise source from 5 mHz to 0.8 Hz.

The room temperature ULE cavity was previously used as the clock laser for the JILA Sr lattice clock [18]. This system has routinely performed at a fractional frequency stability of 1×10^{-16}. Since we have not developed a thorough noise budget for this system, we report only an upper limit on the loss angle.

With the technical noise on the cryogenic cavities being sufficiently low, we can extract a mechanical loss angle at each respective temperature. We assume that the mechanical loss in the parallel and perpendicular directions is identical ($\phi_\parallel = \phi_\perp$) [31, 32]. For the i^{th} mirror, the expression for the fractional frequency PSD arising from coating Brownian noise is then [33]

$$S_y^i(f) = \frac{2k_B T d}{\pi^2 f L^2} \frac{1-\sigma_{sub}^2}{\omega_i Y_{sub}^2} \frac{\phi_c(f)}{Y_c(1-\sigma_c^2)(1-\sigma_{sub}^2)} \times \left[Y_c^2(1+\sigma_{sub})^2(1-2\sigma_{sub})^2 + Y_{sub}^2(1+\sigma_c)^2(1-2\sigma_c)\right]. \quad (1)$$

Here, "c" labels the coating, and "sub" labels the substrate. $\sigma_{c(\text{sub})}$ is the Poisson's ratio, $Y_{c(\text{sub})}$ is Young's modulus, d is the coating thickness, ω_i is the $1/e^2$ beam radius at the i^{th} mirror, and $\phi_{c(\text{sub})}$ is the loss angle. Note that we are allowing for the coating loss angle to have frequency dependence.

With the fits from Fig. 2 and Eq. (1), we derive $\phi_c(f)$ and plot the results in Fig. 4. The results are

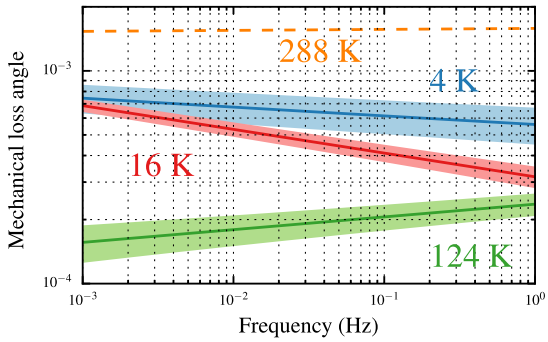

Fig. 4. Frequency-dependent mechanical loss angle for the SiO_2/Ta_2O_5 coatings at different operating temperatures. The shaded bands indicate the 1σ uncertainty.

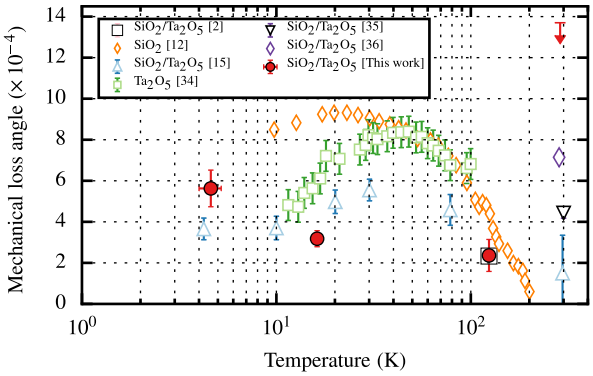

Fig. 5. Mechanical loss of the individual coating constituents (SiO_2, Ta_2O_5), and SiO_2/Ta_2O_5 coatings measured by ringdown (orange diamonds, blue triangles, green squares, purple triangles). Other direct measurements are also included (pink square and black triangle). Our results from direct CTN measurements are shown as the red circles and the red arrow.

$$\phi_{4\,\text{K}}(f) = (5.6 \pm 0.9) \times 10^{-4} \times f^{-0.05\pm0.01}, \quad (2)$$

$$\phi_{16\,\text{K}}(f) = (3.2 \pm 0.3) \times 10^{-4} \times f^{-0.11\pm0.02}, \quad (3)$$

$$\phi_{124\,\text{K}}(f) = (2.4 \pm 0.3) \times 10^{-4} \times f^{0.06\pm0.02}. \quad (4)$$

The shaded band indicates the 1σ uncertainty. We find that the frequency dependence, although rather weak, has the opposite sign at 4 and 16 K compared with the 124 K result. The 4 and 16 K results use mirrors from a different coating run than the 124 K cavity, and so this difference could be coating-dependent.

For comparison with other results published in the literature, we plot ϕ_c as a function of temperature in Fig. 5. The orange diamonds [12], green squares [34], and blue triangles [15] are ringdown measurements that do not explicitly consider $\phi_\perp$ and $\phi_\parallel$. The pink square [2], black triangle [35], and purple diamond [36] are all from direct thermal noise measurements that assume $\phi_\perp = \phi_\parallel$. Our results are plotted at 1 Hz, and no frequency dependence has been assumed for the referenced values, which are largely measured in the kHz frequency range. We measured CTN at several temperatures near 4 K, and average these values together. The x axis error bar for that data point indicates the spread in temperature explored, while the

y axis error bar is the standard deviation of the extracted ϕ_c. We do not see a strong temperature dependence between 4 to 16 K.

We have presented direct measurements of the thermal noise for SiO_2/Ta_2O_5 HR coatings. These measurements are complementary to those attained by ringdown spectroscopy. For the design of future gravitational wave detectors, independent measurements of CTN are important. For ultrastable reference cavities, the use GaAs/AlGaAs crystalline coatings at cryogenic temperatures is important to explore. Other potentially low thermal noise optical coatings could also be tested using cryogenic ultrastable silicon cavities.

Funding. National Science Foundation (QLCI 2016244); Defense Advanced Research Projects Agency; National Institute of Standards and Technology; PTB; Deutsche Forschungsgemeinschaft (EXC-2123 Quantum Frontiers).

Acknowledgment. We thank T. Bothwell, C. Kennedy, and L. Sonderhouse for technical contributions, and to I. Martin and S. Gras for comments on the paper.

Disclosures. The authors declare no conflicts of interest.

REFERENCES AND NOTE

1. T. Kessler, C. Hagemann, C. Grebing, T. Legero, U. Sterr, F. Riehle, M. Martin, L. Chen, and J. Ye, Nat. Photonics **6**, 687 (2012).
2. D. G. Matei, T. Legero, S. Häfner, C. Grebing, R. Weyrich, W. Zhang, L. Sonderhouse, J. M. Robinson, J. Ye, F. Riehle, and U. Sterr, Phys. Rev. Lett. **118**, 263202 (2017).
3. W. Zhang, J. M. Robinson, L. Sonderhouse, E. Oelker, C. Benko, J. L. Hall, T. Legero, D. G. Matei, F. Riehle, U. Sterr, and J. Ye, Phys. Rev. Lett. **119**, 243601 (2017).
4. J. M. Robinson, E. Oelker, W. R. Milner, W. Zhang, T. Legero, D. G. Matei, F. Riehle, U. Sterr, and J. Ye, Optica **6**, 240 (2019).
5. G. M. Harry, H. Armandula, E. Black, D. R. M. Crooks, G. Cagnoli, J. Hough, P. Murray, S. Reid, S. Rowan, P. Sneddon, M. M. Fejer, R. Route, and S. D. Penn, Appl. Opt. **45**, 1569 (2006).
6. J. Cripe, N. Aggarwal, R. Lanza, A. Libson, R. Singh, P. Heu, D. Follman, G. D. Cole, N. Mavalvala, and T. Corbitt, Nature **568**, 364 (2019).
7. K. Collaboration, Class. Quantum Gravity **36**, 165008 (2019).
8. B. Shapiro, R. X. Adhikari, O. Aguiar, E. Bonilla, D. Fan, L. Gan, I. Gomez, S. Khandelwal, B. Lantz, T. MacDonald, and D. Madden-Fong, Cryogenics **81**, 83 (2017).
9. B. P. Abbott and R. Abbott, Class. Quantum Gravity **34**, 044001 (2017).
10. ET Science Team, "Einstein gravitational wave telescope conceptual design study," ET conceptual design study document ET-0106A-10 (2011).
11. E. Oelker, R. B. Hutson, C. J. Kennedy, L. Sonderhouse, T. Bothwell, A. Goban, D. Kedar, C. Sanner, J. M. Robinson, G. E. Marti, D. G. Matei, T. Legero, M. Giunta, R. Holzwarth, F. Riehle, U. Sterr, and J. Ye, Nat. Photonics **13**, 714 (2019).
12. K. Craig, J. Steinlechner, P. G. Murray, A. S. Bell, R. Birney, K. Haughian, J. Hough, I. MacLaren, S. Penn, S. Reid, R. Robie, S. Rowan, and I. W. Martin, Phys. Rev. Lett. **122**, 231102 (2019).
13. I. W. Martin, R. Bassiri, R. Nawrodt, M. M. Fejer, A. Gretarsson, E. Gustafson, G. Harry, J. Hough, I. MacLaren, S. Penn, S. Reid, R. Route, S. Rowan, C. Schwarz, P. Seidel, J. Scott, and A. L. Woodcraft, Class. Quantum Gravity **27**, 225020 (2010).
14. M. Granata, K. Craig, G. Cagnoli, C. Carcy, W. Cunningham, J. Degallaix, R. Flaminio, D. Forest, M. Hart, J.-S. Hennig, J. Hough, I. MacLaren, I. W. Martin, C. Michel, N. Morgado, S. Otmani, L. Pinard, and S. Rowan, Opt. Lett. **38**, 5268 (2013).
15. K. Yamamoto, S. Miyoki, T. Uchiyama, H. Ishitsuka, M. Ohashi, K. Kuroda, T. Tomaru, N. Sato, T. Suzuki, T. Haruyama, A. Yamamoto, T. Shintomi, K. Numata, K. Waseda, K. Ito, and K. Watanabe, Phys. Rev. D **74**, 022002 (2006).
16. G. D. Cole, W. Zhang, M. J. Martin, J. Ye, and M. Aspelmeyer, Nat. Photonics **7**, 644 (2013).
17. G. D. Cole, W. Zhang, B. J. Bjork, D. Follman, P. Heu, C. Deutsch, L. Sonderhouse, J. Robinson, C. Franz, A. Alexandrovski, M. Notcutt, O. H. Heckl, J. Ye, and M. Aspelmeyer, Optica **3**, 647 (2016).
18. M. D. Swallows, M. J. Martin, M. Bishof, C. Benko, Y. Lin, S. Blatt, A. M. Rey, and J. Ye, IEEE Trans. Ultrason., Ferroelectr. Freq. Control. **59**, 416 (2012).
19. M. J. Martin and J. Ye, in *Optical Coatings and Thermal Noise in Precision Measurement* (Cambridge University, 2012), p. 237.
20. W. A. Brantley, J. Appl. Phys. **44**, 534 (1973).
21. R. Nawrodt, A. Zimmer, T. Koettig, C. Schwarz, D. Heinert, M. Hudl, R. Neubert, M. Thürk, S. Nietzsche, W. Vodel, P. Seidel, and A. Tünnermann, J. Phys. Conf. Ser. **122**, 012008 (2008).
22. D. R. M. Crooks, G. Cagnoli, M. M. Fejer, G. Harry, J. Hough, B. T. Khuri-Yakub, S. Penn, R. Route, S. Rowan, P. H. Sneddon, I. O. Wygant, and G. G. Yaralioglu, Class. Quantum Gravity **23**, 4953 (2006).
23. S. Musikant, *Optical Materials: An Introduction to Selection and Application* (Dekker, 1985).
24. K. Numata, G. B. Bianc, N. Ohishi, A. Sekiya, S. Otsuka, K. Kawabe, M. Ando, and K. Tsubono, Phys. Lett. A **276**, 37 (2000).
25. P. Klocek, *Handbook of Infrared Optical Materials* (CRC Press, 1991).
26. K. Numata, A. Kemery, and J. Camp, Phys. Rev. Lett. **93**, 250602 (2004).
27. T. Bothwell, D. Kedar, E. Oelker, J. M. Robinson, S. L. Bromley, W. L. Tew, J. Ye, and C. J. Kennedy, Metrologia **56**, 065004 (2019).
28. A. Amato, G. Cagnoli, M. Canepa, E. Coillet, J. Degallaix, V. Dolique, D. Forest, M. Granata, V. Martinez, C. Michel, L. Pinard, B. Sassolas, and J. Teillon, J. Phys. Conf. Ser. **957**, 012006 (2018).
29. S. Gras and M. Evans, Phys. Rev. D **98**, 122001 (2018).
30. D. Matei, T. Legero, C. Grebing, S. Häfner, C. Lisdat, R. Weyrich, W. Zhang, L. Sonderhouse, J. Robinson, F. Riehle, J. Ye, and U. Sterr, J. Phys. Conf. Ser. **723**, 012031 (2016).
31. Our measurements presented in this manuscript do not distinguish these two loss components. Without loss of generality, we lump them together as a total loss angle. We also note a gradual shift away from the loss angle convention of $\phi_\parallel$ and $\phi_\perp$ in the LIGO community, and the loss angle can instead be defined in terms of bulk loss (ϕ_B and shear loss angles ϕ_S [32]). Approximately, the assumption of $\phi_B = \phi_S$ is equivalent to that of $\phi_\parallel = \phi_\perp$, without detailed treatment of light penetration into the coating layers.
32. T. Hong, H. Yang, E. K. Gustafson, R. X. Adhikari, and Y. Chen, Phys. Rev. D **87**, 082001 (2013).
33. G. M. Harry, A. M. Gretarsson, P. R. Saulson, S. E. Kittelberger, S. D. Penn, W. J. Startin, S. Rowan, M. M. Fejer, D. R. M. Crooks, G. Cagnoli, J. Hough, and N. Nakagawa, Class. Quantum Gravity **19**, 897 (2002).
34. R. Robie, "Characterisation of the mechanical properties of thin-film mirror coating materials for use in future interferometric gravitational wave detectors," Ph.D. thesis (University of Glasgow, 2018).
35. T. Chalermsongsak, F. Seifert, E. D. Hall, K. Arai, E. K. Gustafson, and R. X. Adhikari, Metrologia **52**, 17 (2014).
36. S. Häfner, S. Herbers, S. Vogt, C. Lisdat, and U. Sterr, Opt. Express **28**, 16407 (2020).